1.3 Towards MEMS Probes for Intracellular Recording

Y. Hanein, K. F. Böhringer, R. C. Wyeth, and A. O. D. Willows,
University of Washington, Seattle, WA, USA

Abstract

Simultaneous, multi-site recording from the brain of freely behaving animals will allow neuroscientists to correlate neuronal activity with external stimulation and behavior. This information is critical for understanding the complex interactions of brain cells. Recent interest in microelectromechanical systems (MEMS) and in particular in bio-MEMS research has led to miniaturization of microelectrodes for extracellular neuronal recording. MEMS technology offers a unique opportunity to build compact, integrated sensors well suited for multi-site recording from freely behaving animals. These devices have the combined capabilities of silicon-integrated circuit processing and thin-film microelectrode sensing. MEMS probes for intracellular recording may offer significantly improved signal quality. Here we discuss the basic concepts that underlie the construction of intracellular MEMS probes. We first review the basics of neuronal signaling and recording, and the principles of microelectrode technology and techniques. Progress in MEMS technology for neuronal recording is then discussed. Finally, we describe MEMS probes for intracellular recording, viz., fabrication of micro-machined silicon needles capable of penetrating cell membranes. Using these needles, we recorded localized extracellular signals from the hawk moth *Manduca sexta* and obtained first recordings with silicon-based micro-probes from the *inside* of neurons, using an isolated brain of the sea slug *Tritonia diomedea*.

Keywords: Microelectrodes; Intracellular; Bio-fouling; Microelectrode arrays; Silicon probes; Neurons

Contents

1.3.1   Introduction

Understanding brain structure and function has challenged mankind for many centuries. Only during the second half of the nineteenth century, due to advances in scientific tools and in particular the development of a special staining techniques, did scientists reach the understanding that the brain consists of a complex, interactive network of single cells (neurons). The number of cells varies from $\sim 10^{11}$ in humans down to a few hundred in small invertebrates such as leeches. These networks interact and enable living creatures to function, decide, learn, remember, and achieve consciousness. In recent decades, with the rapid development of neuroscience techniques, researchers have obtained detailed information about the function and organization of the brain, and the structure (Figure 1.3-1) and operation of neurons.

Modern tools to investigate the brain consist of a wide variety of techniques such as positron emission tomography (PET) scanning, functional magnetic resonance imaging (fMRI), and electrical recording, among others. Each of these tools is optimized for specific applications. Different techniques may complement each other and several techniques may be used simultaneously. Existing techniques fall into many categories, such as invasive versus noninvasive, local versus regional, and therapeutic versus research. Clearly, for diagnosis purposes a

Figure 1.3-1. An immunolabelled brain of *Tritonia diomedea* (sea slug). Different dyes are used to mark cells that contain different neurotransmitters, specific chemicals used by neurons to communicate with each other. It is important to note that only a fraction of the cells are stained and so the stained cells appear on an unstained background, that is actually filled with other cells. Image by Jim Beck.

noninvasive technique is preferred and a system such as PET scanning, a noninvasive imaging procedure that visualizes local changes in the cerebral blood flow, has established itself as a standard diagnosis tool. Despite the wide variety of existing tools and despite the great progress of the recent years, many questions related to brain activity are still unresolved and principles that underlie many brain processes are still unknown. It is widely acknowledged that further progress will be enhanced by novel probing tools.

Neuroscience has accomplished much in understanding how individual neurons function and how they work together in small populations. However, much less is known about how different parts of the nervous system are integrated. For example, how are the different senses used to navigate through the environment? This type of question exceeds the capabilities of current tools. Conventional tools require extensive laboratory apparatus, and eliminate the normal sensory world. In order to understand nervous system function at the system level, we need to reduce the influence of laboratory apparatus. An unencumbered setting allows animals to have real sensations and feedback from their own activities.

A better systems-level recording tool will allow researchers to perform high-fidelity multi-site intracellular recording from freely behaving animals. This will allow neuroscientists to study the correlation between (a) neuronal activity and external stimulation and (b) neuronal activity and behavior, and also to understand better the communication patterns inside neural networks. As we will show below, existing intracellular probes are well suited for studying the physiology and the processes of *single, living* cells, in particular for understanding heteroge-

neous living cell populations that make up dynamic systems such as neural networks. However, despite their obvious advantages, existing intracellular probes are usually large, bulky, fragile, and not available in arrays.

Microelectromechanical systems (MEMS) technology may provide an opportunity to develop multi-site recording from freely behaving animals. MEMS offer small overall dimensions, easily prepared arrays, and built-in integrated circuit capabilities [1]. Recently, researchers have demonstrated the capabilities of planar microelectrode array (MEA) probes to study specific neurological problems [2, 3].

This chapter reviews the basic principles of intracellular recording and describes the motivation and challenges associated with the fabrication of intracellular MEMS probes. We begin our discussion with a short review of neuronal structure and activity. We then discuss neuronal signals and how these signals are recorded. We dwell on the properties of different recording elements and in particular on microelectrodes. The differences between extra- and intracellular recording are presented and discussed. We then discuss MEMS electrodes and the techniques used in their construction. Finally, we present the details of MEMS-based intracellular probes that we have constructed recently. Using these needles, we now obtain extremely localized extracellular signals and have made first recordings with silicon-based micro-probes from the *inside* of neurons.

1.3.2   Principles of Neuronal Recording

Neuronal communication is at the core of brain activity, and understanding its signaling is the key to understanding how the brain works. Many neuroscientists therefore wish to be able to record these signals in real time and from large numbers of neurons simultaneously. To understand neuronal recording we first need to clarify some of the basic conceptual and structural issues related to the brain. A good starting point is understanding individual electrically excitable brain cells (ie, neurons) and their connectivity. A comprehensive description of these processes can be found elsewhere [4–7]. Here we briefly summarize the basic principles.

1.3.2.1   Neurons

Neurons consist of a cell body, axons, and dendrites all enclosed by a thin, fragile, phospholipid bilayer membrane (Figure 1.3-2). The signals generated by neurons are transmitted by their axons to synapses at their terminals. These terminals usually contact dendrites or the cell body of another neuron (post-synaptic neuron). The inputs to a neuron are often delivered by chemicals (neurotransmitters) diffusing across one or many synapses from presynaptic neurons.
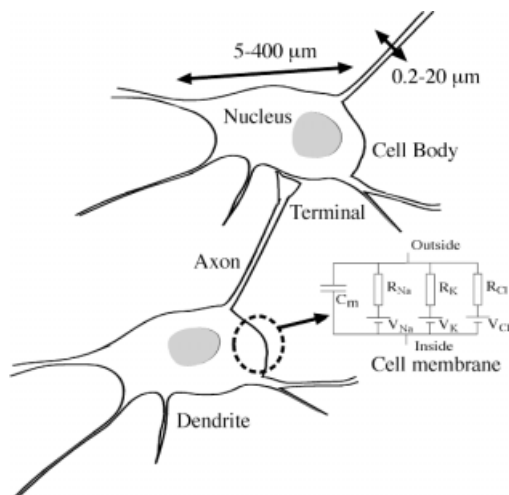
Figure 1.3-2. Neuron structure. Dendrites and the cell body receive 'inputs' across synapses, and the axon sends signals on to other neurons across synapses at its terminals. The cell membrane is a thin insulating layer that separates two conducting layers (the interior and the exterior of the cell). Therefore, the membrane can be regarded as a capacitor with additional potential sources and resistors representing the different ionic channels in the membrane. A simplified electrical equivalent circuit of the membrane is shown in the inset following the well-known Hodgkin-Huxley approach. According to this model a neuron can be represented by an electrical equivalent circuit that includes elements representing different membrane components. Many of the mechanisms underlying these components are now well understood.

The chemical signals are transduced into electrical signals, which are regenerated actively along the cell membrane. These signals, whether arising on dendrites or the cell body, may culminate in another regenerative electrical membrane impulse, transmitted along the axon to the terminals. Again, the impulse causes release of neurotransmitters that diffuse across the synapse to the next neuron, and the cycle repeats. Direct electrical communication not mediated by chemicals is also common between neurons. In either case, the impulse traffic and underlying synaptic potentials are central interests of neuroscience. To understand measurement of this bio-electricity we need to proceed one step further into the structure of the cell.

1.3.2.2   Neuronal Signaling

Neurons are surrounded by a semi-permeable membrane. The membrane insulates the conducting interior from fluids surrounding the cell. Ionic pumps in the membrane transport ions from lower to higher electrochemical potential, maintaining electrochemical gradients across the cell membrane. Owing to ionic con-

centration gradients and differential membrane permeability, primarily to K^+, Na^+ and Cl^-, neurons sustain a DC potential (resting potential) across the membrane. This resting membrane potential (V_m) varies for different systems, with typical values of –90 mV for humans, –70 mV for the squid giant axon, and –50 mV for sea slug neurons.

In neurons, the membrane potential is modulated by ionic currents through several different types of ion-specific channels across the cell membrane. These channels can selectively permit different ions to cross the membrane (down their electrochemical gradients). Depending on their timing, location, and ion specificity, ionic movements alter the membrane potential with corresponding rates, amplitudes, and direction.

There are two broad categories of electrical events brought about by these ionic movements: passive and active. A very common example of a passive electrical signal is the post-synaptic potential. Channels on the post-synaptic neuron open in response to the chemical diffusing across the synapse and cause the membrane potential near that synapse to increase or decrease. This voltage change moves *passively* along the membrane, affecting closer areas of membrane more than those more distant. If enough of these small post-synaptic potentials combine in an area of voltage-sensitive channels, then an *active* or regenerative electrical impulse will occur. An active electrical impulse will move along the membrane whenever a changing membrane potential in one area of membrane induces a similar change in membrane potential in an adjacent area. This action potential is a fast and relatively large voltage change, and by actively regenerating itself can travel much farther than passive electrical signals. By propagating along contiguous areas of active membrane, the signal can quickly travel the length of an axon and initiate synaptic transmission to the next neuron. To understand how neurons work, and work together, it is very helpful to record both the small post-synaptic potentials and the resultant transmitted action potentials.

An example of how this process occurs is odor detection [7]. Sensory neuron terminals inside the nasal cavities have extensions with embedded ionic channels. These channels open in response to only a few odor chemicals, creating small 'receptor' potentials, almost identical with post-synaptic potentials. If enough of the specific odor chemical interacts with the sensory neuron terminals, then those small potentials combine additively to reach a certain threshold voltage, triggering a regenerative action potential in the sensory neuron. Different sensory neurons have different types of receptor channels, and thus sensitivity to different chemicals. The combination of receptor potentials and action potentials is used to code the presence or absence of a certain chemical, and the pattern of firing across the whole population of sensory neurons is used to code the odor composition of the air breathed by the animal. Action potentials generated in sensory neurons are transmitted to the brain, where the olfactory information is processed. Perhaps, if the odor is noxious, through a series of synaptic potentials and action potentials, the information will be transmitted to parts of the brain which control movement, allowing the animal to turn its head away from the odor source.

How do neuroscientists observe and understand this process? Fundamentally, there are two ways to record the transmembrane voltages associated with neuron

activity. The intracellular method uses two electrodes: one inside the cell (intracellular electrode), and the other outside (reference electrode). This method records transmembrane signals, ie, post-synaptic potentials and the action potentials (impulses). The other, extracellular method, places two electrodes outside the cell, one very close to the cell and one further away. Although the signals recorded in this way do not strictly measure the transmembrane currents generated by the neuron, any regenerative or other large currents generated nearby the electrodes may cause voltage differences between the two electrodes. Extracellular recording is therefore effective for recording action potentials, but is less likely to detect post-synaptic potentials or other small potential changes. All changes in membrane potential hold information about the way neurons integrate their inputs and communicate their outputs, and by recording and understanding these signals one can observe the basics of brain communication. Let us now turn to the details of the tools one can use to record these signals.

1.3.2.3 Neuronal Recording

Over the past five decades, a wide variety of electrodes have been developed to record bio-electric events. A subclass of these electrodes are small, localized probes typically used to study neuronal signaling [6]. As we will show below, the electrical properties of a microelectrode determine its reliability as a recording transducer. Aspects of design, materials and fabrication may cause distortion, electrical noise, and instability.

Most electrodes are either metallic or glass micro-pipettes [8]. We begin this section with a review of these two most common recording devices and then discuss their two associated alternative recording approaches, viz., intra- and extracellular recording. This discussion will point out the relevant issues in designing a silicon-based probe suited for intracellular recording. Finally, we will introduce planar MEAs.

A straightforward approach to realizing a small, localized probe is to use an exposed tip of a sharp, insulated, conducting wire (Figure 1.3-3b) [6]. In these probes the signal is transferred from the tip through the wire while a dielectric material provides the insulation between the wire and the surrounding environment. An additional standard technique to achieve tips with sub-micrometer dimension is by pulling heated glass capillaries [4] (Figures 1.3-3c and 1.3-4). These pulled micro-capillaries can be easily transformed into microelectrodes by filling them with an electrolyte (typically KCl or KOAc) and placing a Ag/AgCl electrode in the electrolyte. The glass wall (Figure 1.3-4b) provides ionic insulation and ensures virtually no leak current.

Despite a number of significant differences between the metal and micro-pipette electrodes, the underlying principles are similar and have been investigated extensively. In essence, all recording electrodes consist of a metal-electrolyte interface. Unlike the simple ohmic metal-metal contact, a metal-electrolyte contact is a rather complex system [9].
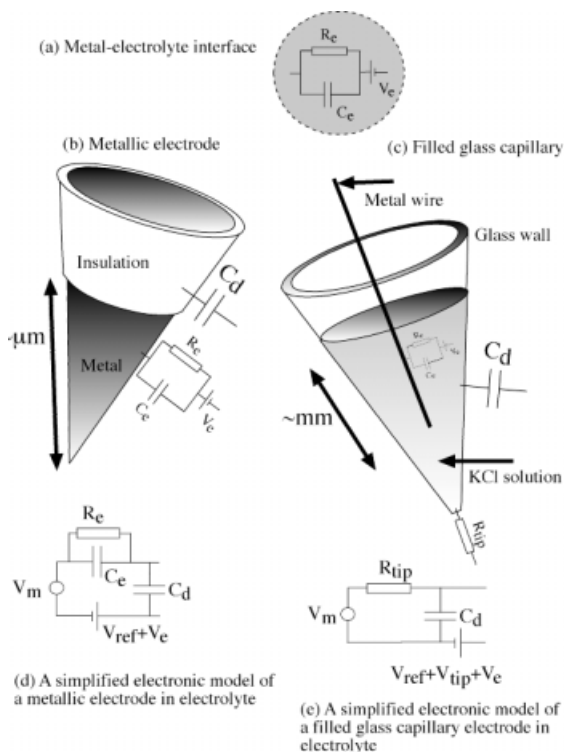
Figure 1.3-3. Bioelectricity-recording electrodes. (**a**) A simplified electronic model for a metal-electrolyte interface. V_e represents the potential drop across the interface, R_e the resistance and C_e the capacitance of the metal-electrolyte interface. This model is used for the metallic and the filled-glass microelectrodes. (**b**) A schematic drawing of a metallic electrode. (**c**) A schematic drawing of a filled glass capillary. (**d**) A simplified electronic model for a metallic electrode in an electrolyte solution. (**e**) A simplified electronic model for a filled-glass capillary electrode in an electrolyte solution. Comparison between the circuits in (**d**) and (**e**) demonstrates the effect of the geometry of the electrode on its electrical properties. In metallic microelectrodes the metal-electrolyte interface is located at the recording tip and therefore accounts for almost all the impedance of the electrode.

Various chemical reactions may take place when a metal is introduced into an electrolyte. These reactions may involve dissolution of the metal in the case of partially soluble metals, or electron exchange between the metal and the solution as in the case of noble metals. The result of these chemical reactions is the formation of an equilibrium charge gradient at the interface (usually referred to as the electric double layer) which is accompanied by a buildup of an electric potential across the interface. The details of the space charge layer are predicted by theoretical models (Helmholtz, 1897), which can then be used to analyze the electrical properties of an electrode.
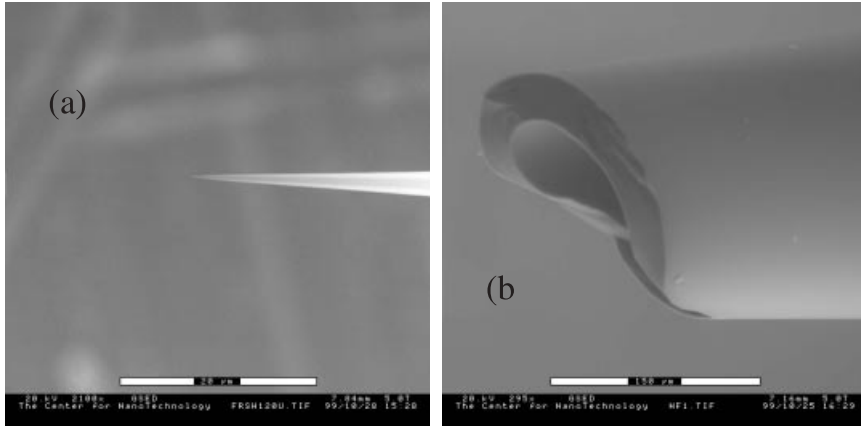
Figure 1.3-4. Glass micropipettes. (**a**) An Environmental scanning electron microscope (ESEM) image of the tip of a pulled glass capillary. The scale bar is 20 μm. Similar tips are commonly used for intracellular neuronal recording. (**b**) An ESEM image of a broken glass capillary. The glass provides superb insulation between the inner and the outer sides of the probe. The scale bar is 150 μm.

Owing to the capacitive nature of the electric double layer, a metal-electrolyte interface is, in fact, an electrolytic capacitor (eg, for platinum $C_e = 20$ μF/cm^2 at 1 kHz). In addition to the capacitive nature of the metal-electrolyte interface, we should also consider its resistive nature. A metallic electrode and an electrolyte maintain equilibrium potential and a balance between influx and efflux currents of electrons (or ions). By applying an external potential, the equilibrium current is unbalanced, and the induced current can then be expressed [10] by

$$i = i_0 e^{F\Delta V/2RT} - i_0 e^{-F\Delta V/2RT} \tag{1}$$

with i_0 being the exchange current density (values may range from pA/cm^2 up to 10 A/cm^2), ΔV is the applied potential, F the Faraday constant, R is the gas constant, and T is the temperature. For small voltages, Equation (1) can be linearized and expressed as

$$i = i_0 F/RT \Delta V \ . \tag{2}$$

At room temperature the electrode resistance (typically denoted as the charge transfer resistance) can be expressed as $R_e = \Delta V/i = 0.06/i_0$. For platinum, $i_0 = 4.5 \times 10^{-6}$ A/cm^2, which corresponds to $R_e = 1.3 \times 10^{12}$ Ω/cm^2. Clearly, for very small electrodes the above expression results in very significant resistances, which are in many cases one of the major complications in the construction of metallic electrodes.

In practical terms, the space charge layer at the metal-electrolyte interface can be simply modeled as a voltage source (V_e) in series with a capacitor (C_e) and a resistor (R_e) in parallel (see Figure 1.3-3 a) (this model is appropriate for low fre-

quencies; at high frequencies the impedance can be modeled by an equivalent circuit of resistor and capacitor in series [10]). For many materials, the values of the simplified components have been determined [10, 11]. It is important to note that these elements cannot be treated as a capacitor or resistor with fixed values. In fact, the values of these elements vary with frequency [10, 12, 13] and also with material, electrolyte, and temperature. This dependence reflects changes in the double-layer properties with these parameters.

Let us begin with analyzing the properties of metallic recording electrodes (for detailed explanations, see [11]). It should be noted that the intracellular MEMS probes, which we fabricate, are very similar to these probes. In Figure 1.3-3b we draw a schematic presentation of an electrode. We also illustrate the major electrical components. The electrode consists of two components: a metallic tip and an insulated shank. The metallic tip can be represented (when placed in an electrolytic solution) by a resistor (R_e), a capacitor (C_e), and a potential source (V_e). The insulation of the electrode shank separates the metallic conductor of the electrode from the conducting electrolytic solution and therefore can be simply represented (when placed in electrolytic solution) as a capacitor (C_d). Additional components in the system are the shank and electrolyte resistances (determined by the geometric surface area of the tip [10, 12]). The equivalent electric circuit of such a probe in recording conditions (with a reference electrode) is shown in Figure 1.3-3d and follows directly from the model in Figure 1.3-3a. Note that some elements, such as the resistance of the electrode shank, and the intra- and extracellular liquid resistances were omitted as they are negligible in comparison with the other elements in the circuit.

The equivalent electrical circuit for the micro-pipette electrodes is shown in Figure 1.3-3e. Here, too, we can neglect various elements. In this example the metal-electrolyte resistance and capacitance (R_e and C_e) are negligible owing to the large surface area of the contact between the electrolyte and the wire. The two major components that determine the electrode impedance are the electrode resistance (R_{tip}) and the glass wall capacitance (C_d). The first is the resistance of the electrolyte through the narrow tip opening, and is determined by the tip diameter. The capacitance is determined by the glass wall thickness.

If we compare Figures 1.3-3d and 1.3-3e it becomes apparent that the geometric differences between the two electrodes produce significant electrical differences. In metallic microelectrodes the metal-electrolyte interface is located at the recording tip and therefore accounts for almost all the impedance of the electrode. The electrical properties of a micro-pipette are dominated by the glass tip resistance. Typically, glass micro-pipettes have DC resistances in the order of 10–200 MΩ, while metallic electrodes may have DC resistance larger by at least two orders of magnitude. On the other hand, in AC, metallic electrodes outperform micro-pipettes which may poorly represent rapidly changing signals owing to their large shunt capacitance. These differences can have a direct impact on the performance of the electrodes for different applications [13]. For example, the electrolyte-filled electrodes will perform as low-pass filters. Therefore, they are most suited for intracellular recording of relatively slowly changing potentials. On the other hand, the metallic electrodes act as high-pass filters, which

suggests their use for more rapidly changing signals. The impedance of the electrode (determined by the materials and geometry) and the impedance of the external path determine the amount of distortion of the recorded signal [13, 14]. Careful choice of metallic electrode parameters can significantly improve their DC performances, their stability, and their distortion.

By considering the differences between metallic electrodes and micro-pipettes, we can explain the parameters and considerations which are related to the design of recording electrodes. Let us now turn to explain when and how these parameters become relevant in an experiment. The performance of an electrode is largely determined by the event under investigation (ie, rapidly or slowly changing signals) and by the anatomical location. Recordings can be made with the electrode inside or outside the cell. Clearly, placing electrodes inside the cell imposes some major challenges on the construction and handling of the electrodes. However, there are several major drawbacks to extracellular recording that make intracellular recording worthwhile. First, information gathered by extracellular sensing may not be exclusive to a single cell (this statement is valid for the case of poor sealing between the electrode and the cell membrane; see the discussion below). Rather, it may be an average over several cells located at the vicinity of the probe. Second, extracellular probing does not provide critical information about DC conditions or slowly changing potentials across the cell membrane. Only the time of occurrence of action potentials can be recorded, not the details of their form. This is a direct result of the capacitive nature of the cell membrane (typical values of the order of 1 $\mu F/cm^2$).

To understand these differences better, we present in Figure 1.3-5 a comparison between extra- and intracellular recording results. The recording was from an isolated brain of *Tritonia diomedea. Tritonia* is a marine mollusk indigenous to the Pacific Northwest; its hallmarks are extraordinarily large brain nerve cells (see Figure 1.3-1), identifiable sensory and motor functions associated with these brain cells, and robust response to surgical insult. Brain preparation methods for this animal allow recording and stimulating a brain during voluntary and reflexive movement [15].

Two electrodes were used to record simultaneously from the same neuron. The first electrode was an intracellular electrode inserted into the neuron. The second extracellular electrode was placed directly adjacent to the first electrode and suction was applied to seal the electrode against the edge of the brain, directly over the cell. Although both records show the action potentials, the dynamic range of the intracellular recording is roughly three decades larger than that of the extracellular recording. Missing from the extracellular record are both the action potential shape and DC changes in the resting potential (here induced by positive and negative current injection). With higher amplification, small synaptic potentials which are clearly visible in the intracellular record, are invisible in the extracellular record. In an extracellular recording, a nearby-firing neuron can confound and sometimes obscure action potentials from the cell of interest; this effect never occurs in intracellular recordings.

To conclude our discussion so far, intracellular recording is important when one wants to know more than just when a neuron fired (and even then, extracel-
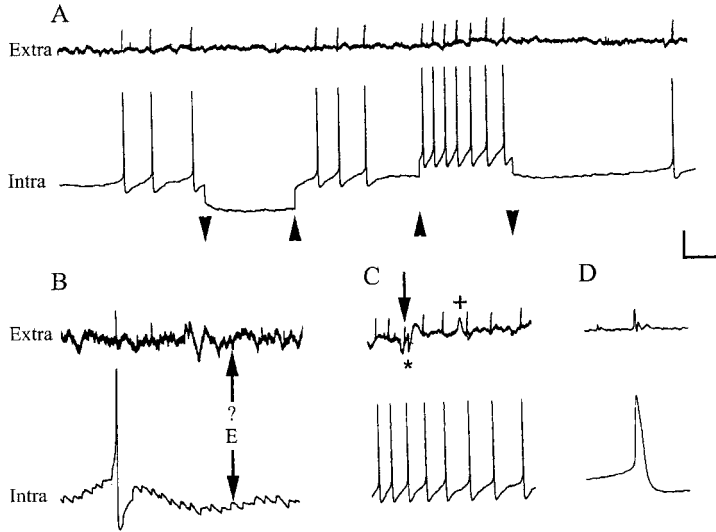
Figure 1.3-5. Extracellular and intracellular recordings from a single reidentifiable neuron, in an isolated *Tritonia* brain. An intracellular electrode was inserted into the neuron. An extracellular electrode was applied with suction, directly nearby. (**A**) Although both records show the action potentials, the dynamic range of the intracellular recording is roughly three decades larger than that of the extracellular recording. Missing from the extracellular record are both the action potential shape and the DC changes in the resting potential (here induced by positive and negative current injection (arrowheads), but also occurring *in vivo*). (**B**) With higher amplification, small synaptic potentials (eg, excitatory post-synaptic potentials, one marked by **E**) clearly visible in the intracellular record, are obscured in the extracellular record. (**C**) In an extracellular recording, a nearby-firing neuron can confound and sometimes obscure action potentials from the cell of interest (arrow); this effect is absent from the intracellular record. (**D**) A single action potential shown on an expanded time-scale. Analyzing an extracellular record is clearly more difficult than analyzing an intracellular record. Scale bar: (**A**, **C**) extracellular 25 μV, 5 s; intracellular 25 mV, 5 s; (**B**) extracellular 10 μV, 5 s; intracellular 10 mV, 5 s; (**D**) extracellular 25 μV, 0.2 s; intracellular 25 mV, 0.2 s.

lular recordings are hard to associate with a single, identifiable neuron). Intracellular recordings are useful to observe the full electrical activity of single neurons: the small DC changes associated with synaptic interactions, the shape of action potentials (which can also be critical), and the timing of action potentials. For these reasons, our goal is to build a silicon-based intracellular electrode. Therefore several requirements are imposed. Special attention has to be directed not only to their geometry but also to the fidelity of the probes under DC and AC conditions. Our silicon-based electrodes should have performances similar to those of the intracellular micro-pipettes. It is very important to emphasize that the extracellular recording we discussed above was performed with a tight seal and therefore represents the best case scenario for extracellular recording.

To summarize, here are some topics that must be considered in the design of silicon-based intracellular probes. Special attention has to be directed to possible instability and noise sources. Stability can be improved by adequate choice of metal. It is widely accepted that silver/silver chloride electrodes are the most stable electrodes [11, 14]. When discussing microelectrodes we should also consider the following two main sources of noise. The first is associated with the unstable metal-electrolyte interface. Here too, the noise level is determined by the metal used. However, this noise may also be dramatically affected by the preparation procedure (ie, the exact parameters of chloriding) as well as the final hookup to the measurement apparatus. A second noise source is thermal noise. Thermal noise effects are related to the resistance of the probe and can be minimized by reducing the electrode impedance. An additional major source for artifacts is the amplification stage. Incompatibility between the probe and the amplifier may distort the signal. Finally, to minimize galvanic potentials, a reference electrode of the same metal as the recording electrode should be used.

1.3.2.4   MEMS Neural Probes

Owing to the multicellular nature of the nervous system, simultaneous recording from a large number of neurons may be helpful. MEMS devices are particularly promising for achieving this goal owing to their small dimensions and the ease with which multi-site devices can be produced. Indeed, extensive effort in the past three decades has shown the potential of planar MEA devices for neurological and electrochemical sensing applications.

What is MEMS and what makes MEMS such an appealing technology for neurological applications? MEMS technology takes advantage of micro-fabrication techniques to construct a wide variety of small electromechanical and also chemical and biological devices [16]. The number of existing techniques, such as metal deposition, bulk etching, dielectric deposition, and molding, is so vast nowadays that the miniaturization of various tools and devices is becoming an everyday reality. MEMS technology has become dominant during recent decades in various applications such as accelerometers, digital mirror displays, and DNA chips.

Silicon-based planar microelectrode arrays were developed with the forethought to allow both *in vivo* and *in vitro* multiple site recording. These devices support the combined capabilities of silicon integrated-circuit processing with thin-film microelectrode sensing. The pioneering work by Wise et al. [18] has been followed by numerous studies that exploited integrated-circuit technology to build neurological microelectrodes. These devices typically consist of metallic electrodes, such as iridium [17], gold [19, 20], and platinum [21], which are photolithographically patterned on passivated silicon substrates (Figure 1.3-6). The interconnects are passivated by a dielectric layer. The *in vivo* designs include a release process that separates needle-shaped devices from the silicon wafer. For a review on the design and realization of thin-film microelectrodes, see [12].
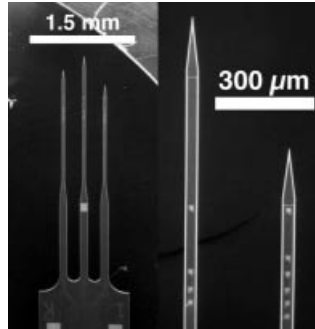
Figure 1.3-6. Silicon-based planar microelectrode arrays (MEAs) for cortical recording. D. Kewley and G.T.A. Kovacs. By permission.

An additional benefit of MEMS devices is the wide variety of additional sensors or effectors that can be integrated with the recording electrodes. With such elements neuronal recording can be linked with chemical stimulation using fluidic channels and valves [22], or temperature control using micro-heaters [23].

Thin-film microelectrodes are produced using standard micro-machining processes. Even though most of these techniques were originally developed for the silicon microelectronics industry, and may include the use of some very harsh chemicals, completed devices made of silicon, noble metals, and dielectric layers, such as silicon dioxide, nitride, or polyimide, are not toxic and can be successfully used to interface with biological elements. A very detailed study by Kristensen et al. [24] demonstrated that the coupling between brain tissues and silicon-based chips had little effect on the tissue under investigation. However, the overall compatibility of the device with the biological environment includes several other factors that have to be considered. (Bio-compatibility is a very common term to describe a proper interface between a biological system and a foreign element. However, this is a very broad and often a very poorly defined concept. To avoid ambiguity, we choose to discuss several specific issues which relate to the interaction between implants and biological systems.)

The first issue is bio-fouling, ie, the strong tendency of proteins and organisms to adsorb physically to synthetic surfaces [25]. Bio-fouling by bacteria is a major source of failure for scores of devices, including macroscopic-scale elements such as metal piping [26]. In the microscopic world of MEMS, bio-fouling is a very challenging issue and adsorbed proteins are known to clog devices with small constrictions, such as bio-capsules [27].

The driving mechanism for bio-fouling in live organisms is protein attachment. This process may affect various devices such as pH [28] and glucose [29] sensors. In these cases, the adsorbed protein layers directly affect the operation of the sensor. Protein layers are also responsible for various biological responses, such as cell attachment and activation [30]. Cell attachment may interfere with the optimal operation of the device by, for example, reducing its life span or increasing its power consumption [31].

Protein and cell attachment to a device surface may trigger the response of the immune system, which in turn may result in inflammation. It is therefore important to consider not only the short-term effects of the biological environment on the device (the effects of protein adsorption on electrode performance are known to occur during periods of hours [28] or days [29]) but also the longer-term effects of the device on the hosting environment. It is important to note that these effects may vary for different applications and biological systems.

Clogging of micro-pipette intracellular electrodes over several hours suggests that protein adsorption may interfere with the recording. In the case of metallic intracellular electrodes, the tips are exposed to protein adsorption. This may affect the recording stability. The components of the device outside the cell are also susceptible to cell attachment. To resolve these problems, surface modification techniques [27, 32] can be integrated with standard MEMS processes and can dramatically reduce protein and cell attachment. It has also been shown that a thin non-fouling coating may provide protection to coated electrodes from protein adsorption and cell attachment without compromising their conductivity [32].

Another major problem related to the interface between artificial devices and biological environments is corrosion. Direct contact between the device and the biological system exposes the surface of the device to corrosive aqueous media. The durability of the device is therefore strongly dependent on the properties of the passivation layer and the quality of the adhesion of the different coatings on the device. Passivation layers used in microelectrode fabrication, such as silicon dioxide, silicon nitride, or polyimide, were originally developed as dielectrics for non-corrosive environments and therefore may perform very poorly (failure after several minutes or hours) in electrolyte solutions. The use of these passivation materials for corrosive environments requires special attention. By studying a large number of common barrier materials as a passivation layer for silicon-based microelectrode devices, Fassbender et al. [33] demonstrated that by a careful choice of material and preparation the corrosion resistance of the passivation layer can be maintained for several months. It was shown that by adequate control of deposition conditions and process cleanliness, effects such as stress, pinholes, and particle inclusion were avoided. In return, effects as buckling and swelling were dramatically reduced and the overall corrosion resistance of the devices was improved.

A major consideration in the design of microelectrodes is their geometric interface with the environment. As was briefly mentioned before, a tight seal between the electrode and the cell membrane is favorable for good extracellular recording. These conditions are very hard to reach with flat electrode designs and a special effort was made, in *in vitro* setups, to improve the sealing by shaping the electrode sites into a cup structure [34]. Action potential simulations based on the equivalent electric circuit of neuron-to-electrode contact show significant signal distortions due to inadequate sealing [35, 36]. Clearly, good sealing is very hard to realize *in vivo* with thin-film microelectrode devices and therefore, despite their many appealing advantages, their recording capabilities are limited to applications where the understanding of synaptic interactions is important.

It is important to note that complete sealing between the recording electrode and the cell membrane may not always be a major problem. This may depend on the level of detail that one requires from the recording and also on the exact experimental setup, ie, whether the recording is performed with brain cells or other nerve cells. MEMS surface electrodes, even without complete sealing, can be used to study brain activity of intact and freely behaving animals [2, 37]. The signal-to-noise level is sufficient to allow spike detection and sorting.

Improvement of the signal-to-noise ratio and higher signal amplitude can be achieved by fabricating three-dimensional tip-shaped electrodes (tips extending from the two-dimensional surface of the wafer). Such designs allow electro-physiological recording from inside a cultured tissue [24, 38]. Campbell et al. [38] used thermo-migration to define p-doped columns in n-doped substrates. A dicing saw was used to define pillars in the p-doped regions. This process allows the formation of tall, electrically insulated pillars. The pillars were sharpened by a chemical etch consisting of 5% hydrofluoric and 95% nitric acid. Gold and platinum were deposited on the tips with a metal foil used as a protection mask for the base of the electrodes. Thiébaud et al. exploited the anisotropic etching characteristics of silicon in KOH to form 47 μm tall tips [39]. The tips were passivated, and then deposited with platinum. As in the planar microelectrode case, the metal is passivated with an additional dielectric layer. A thick photo-resist was patterned and used as a mask to expose the electrode tips.

Owing to the advantages of intracellular recording mentioned above, combined with the favorable properties of MEMS as an enabling technology for neuronal recording, the development of intracellular MEMS probes appears to be a promising approach and is the focus of the current study.

1.3.3   Intracellular Neural MEMS Probes

As was discussed in Section 1.3.2.3, pulled glass capillaries electrodes are most suited for DC recording. MEMS probes based on a similar design, namely hollow capillaries [40], may be ideal for such recording but their realization may be difficult. Needle-like electrodes based on rigid, metallized tips suited for intracellular recording require close attention to their DC properties, but their realization may be more feasible than hollow electrodes. In fact, needle array devices have already been realized and used for extracellular recording [38, 39].

The focus of the current study is the fabrication of micro-machined silicon solid needles suited for intracellular probing. Our main effort has been directed towards the construction of tips capable of penetrating the cell membrane as well as optimization of the electronic properties in DC.

We discuss below the main consideration in the design of these probes. We then describe the fabrication steps including initial characterization and optimization of the different components. To demonstrate the probe performances, we used two biological models: *Manduca sexta* (hawk moth) and *Tritonia diomedea* (a sea slug). Our results indicate that the electrodes act as extremely localized bio-sensors.

1.3.3.1 Tip Design

In Section 1.3.2.3, we discussed the parameters required to model and understand microelectrodes. In this section we discuss the specific design of the MEMS electrodes we produce and estimate the typical values of the different components. The discussion is followed by the fabrication details.

A major challenge in producing probes for intracellular sensing is the tip geometry. Intracellular probes must have extremely sharp tips (sub-micrometer dimensions) and they have to be long ($> 10 \, \mu m$). These characteristics are necessary for effective bending and penetration of the flexible cell membrane.

The structure of our electrodes is based on solid silicon needles with a conducting silicon base (Figure 1.3-7a). The surface of this structure is then coated with a metal that forms the metal-electrolyte interface (Figure 1.3-8b). A dielectric layer is used to insulate the base of the needle from the electrolyte (Figure 1.3-8c). The insulation has to cover all parts of the electrode other than the very tip. Connection to the electrode is achieved by wiring an insulated conducting wire to the back of the conducting silicon base. The backside of the electrode and the connection to the wire are finally insulated with a thick encapsulation material.

The geometric structure and the properties of the materials used to construct the needles determine their final performances. Let us estimate the low-frequency values of the different components in this circuit. We begin with the metal-electrolyte interface. The interfacial capacitance (C_{tip}) can be estimated by

$$C_{\text{tip}} = C_{\text{e}} A_{\text{tip}} \; . \tag{3}$$

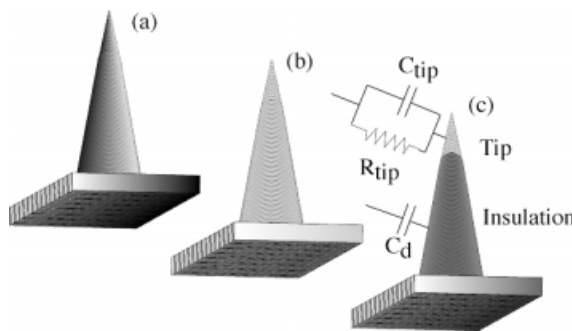The charge transfer resistance (R_{tip}) can be estimated by the following simple calculation:

Figure 1.3-7. Schematic drawing of the MEMS intracellular electrodes used in this study. (**a**) The electrodes are made of sharp, bare, silicon needles; (**b**) the bare silicon is then coated with a metal; (**c**) finally, a dielectric passivation layer is deposited on the metal layer and the tip of the metal is exposed. The simplified electric model for the tip and the insulation are also presented. The justification to this simplified model is detailed in the text.
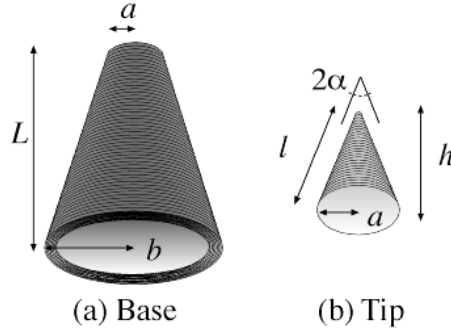
(a) Base   (b) Tip

Figure 1.3-8. Schematic drawing of the MEMS intracellular electrodes. (**a**) Geometry of the base, (**b**) geometry of the tip.

$$R_{\text{tip}} = R_{\text{e}}/A_{\text{tip}} \tag{4}$$

where C_{e} and R_{e} are the specific capacitance and resistance of the metal-electrolyte interface respectively, and A_{tip} is the tip area. In order to maximize the capacitance and minimize the resistance, we need either to increase the effective area of the electrode or to choose a material with high specific capacitance and low charge transfer resistance. A standard way to increase the effective area is by using rough and porous materials, such as porous silicon [41] or platinum black, which can be electroplated on the surface of the electrode [10]. Another alternative to reduce the impedance of the electrodes is to use a material with high specific capacitance such as silver chloride. Silver can be easily deposited by thermal evaporation and chloridation can be achieved by several post-processing means. The details of the chloridation process are discussed below. The estimates below are made for silver/silver chloride electrodes. Noble metal electrodes, such as gold electrodes, would present inferior performances.

For a conical geometry (Figure 1.3-8) the effective area is given by the radius a and the length l:

$$A_{\text{tip}} = \pi a l \;. \tag{5}$$

For $2a = 9°$ and $h = 20$ μm, $A_{\text{tip}} \approx 100$ μm^2. With typical values of $C = 100$ μF/cm^2 (Ag/AgCl), $C_{\text{tip}} \approx 100$ pF. For silver chloride electrodes the frequency dependence may be roughly approximated by $C \propto 1/f^{0.4}$, with f being the frequency [11].

To estimate the resistance we can use $R_{\text{e}} = 10^{10}$ Ωμm^2 (for 10 Hz). This value may vary with chloride deposition and can be up to an order of magnitude larger [11]. For $A_{\text{tip}} \approx 100$ μm^2, $R \approx 10^8$ Ω. The values used here are for large electrodes, miniaturization of the electrode could affect the effectiveness of the diffusion of the soluble ions close to the electrode tip and may reduce the effectiveness of the electrode.

We now turn to verify the additional components in the circuit. The resistance of the silicon base can be estimated as follows. The resistance of a truncated cone with radii a and b, a length L, and a resistivity ρ is given by

$$R = \rho L/\pi ab \ . \tag{6}$$

For $L = 400$ μm, $a = 1.5$ μm, $b = 35$ μm and $\rho = 0.0045$ Ωcm, $R = 110$ Ω.

The resistance of the metallic coating deposited on the truncated cone can be estimated as follows

$$R = \rho L/2\pi d \times \ln(b/a)/(b-a) \tag{7}$$

where ρ is the metal resistivity (typical values are on the order of 10^{-6} Ωcm) and d is the metal layer thickness. With $d = 100$ nm, $R = 3\Omega$. The resistance of the metallic coating is comparable to the resistance between the tip and the base. These resistances and also the wiring resistance and the contact resistance is of the same order of magnitude and are low enough to be neglected.

The capacitance of the electrolyte through a passivation layer can be roughly estimated using the parallel plate capacitor equation:

$$C_d = \varepsilon_0 \varepsilon_r A_{Base}/d_d \tag{8}$$

where ε_0 is the dielectric permittivity of free space, ε_r is the relative dielectric permittivity of the passivation layer (for silicon nitride, $\varepsilon_r = 7.5$), and A_{Base} and d_d are the area and the thickness of the passivation layer, respectively. For $A_{Base} = 0.25$ mm^2 and $d_d = 50$ nm, $C = 250$ pF. In the present design the capacitance of the needle shank is negligible compared with the capacitance of the electrode base and can be neglected. In this example, the shunt capacitance may impose undesired perturbations on the proper function of the electrode. To minimize these effects, it is important to lower the surface area and to increase the thickness of the passivation.

To conclude, the needles can be modeled by the circuit in Figure 1.3-3 d. The values for R_{tip}, C_{tip} and C_d can be estimated as 10^8 Ω, 100 pF and 250 pF, respectively. This simple calculation gives a possible range of parameters for metallic electrodes for our current design. Further improvement of the design and the preparation may improve these values. It is also important to consider these values with respect to the choice of other components in the circuit, in particular the choice of the amplifier. The value for R_{tip} is comparable to the typical values of glass capillaries and should allow reliable DC recording.

1.3.3.2 Tip Fabrication

To fabricate needles suitable for intracellular recording, we used highly conducting (n-type), 800 μm thick silicon wafers. Similar to the process in [38] we used a dicing saw to dice the wafer in two perpendicular directions to create arrays of tall pillars ($70\times70\times350$ μm). To sharpen the tips we used reactive ion etching (RIE) with SF_6. This is a robust, self-sharpening process, which we optimized in order to obtain long tips with a high aspect ratio. The process requires approximately 45 min and results in sharp, high aspect ratio needles (Figure 1.3-9).
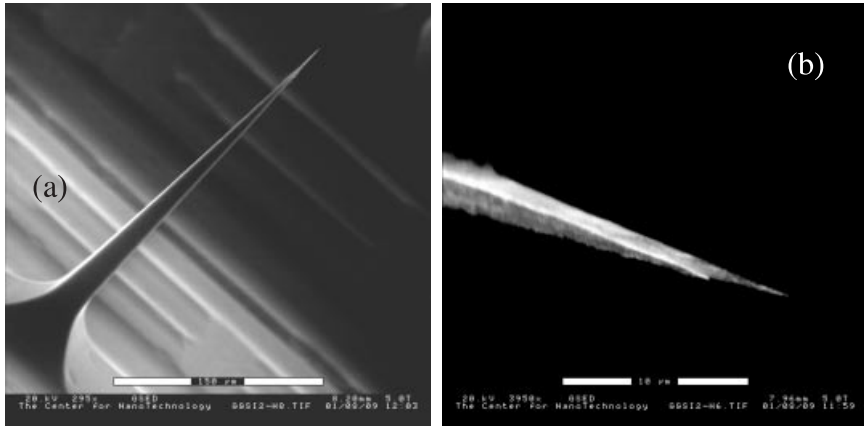
Figure 1.3-9. (**a**) A single needle after the RIE sharpening process. The scale bar is 150 μm. (**b**) A tip of a sharpened silicon needle. The needle is tilted approximately 45° with respect to the plane of the image. The scale bar is 10 μm.

Figure 1.3-9 b shows the tip of a silicon needle that we produced with the process mentioned above. Our process yields a probe geometry that is similar to that of the pulled glass electrodes commonly used in intracellular recording schemes (see Figure 1.3-4 for comparison).

To produce separated needles, the wafer was bonded with crystal bond (or photoresist) to another substrate and cuts to separate the parts were made prior to the sharpening process (Figure 1.3-10). These cuts are approximately 500 μm apart. After the sharpening, the wafer was sputtered with Cr/Au ($\sim$70 nm) and with silicon nitride ($\sim$130 nm). Later, using an RIE SF_6 process, the nitride
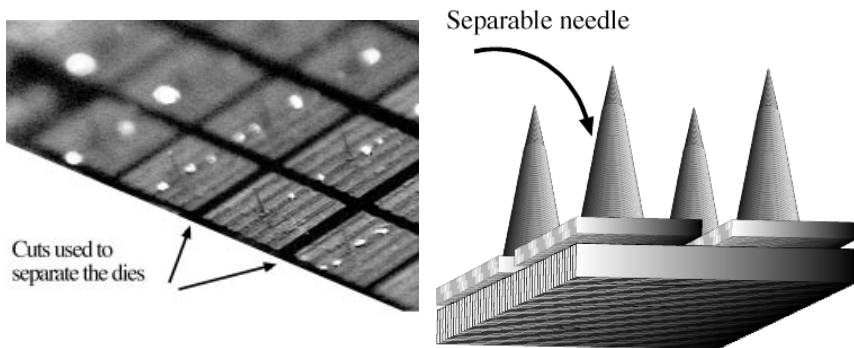

Figure 1.3-10. (**a**) An optical microscope image of an array of diced electrodes. The electrodes are glued to a substrate with an adhesive (photoresist). By soaking the sample in acetone the dies can be separated and used as individual probes. (**b**) A schematic drawing of the electrodes after the sharpening process is completed.

layer was slightly etched in order to expose the needle tips. Finally, we soaked the wafer in acetone and released the single needles.

1.3.3.3   Metallization

The main motivation in performing intracellular recording is to be able to measure slowly varying signals. Thus, intracellular recording is reliable and advantageous only if the probe provides a stable recording. The use of metallic electrodes for DC recording is very challenging. One of the main tasks of our study was to investigate the performance of the electrodes and to explore metallizations best suited for DC operation. We investigated two metallization procedures: gold and silver chloride electrodes. The deposition of gold and silver is easily achieved by thermal evaporation with a thin layer of Cr acting as an adhesion promoter.

Gold, as a noble metal, ensures minimal solubility but may result in very high DC resistance and unstable recording. Ag/AgCl electrodes are commonly used to ensure high stability in physiological probing including in MEMS devices [42]. It was suggested that even the reliable Ag/AgCl electrode may fail to support very high fidelity recording. This may be due to interactions between the silver and organic molecules or to the effect related to miniaturization of Ag/AgCl electrodes [13]. Our results, discussed below, show a dramatic improvement of electrode stability and resistance by using Ag/AgCl electrodes.

1.3.3.4   Silver-electrode Chloriding

The performances of silver chloride electrodes depend very strongly on the preparation process. A rigorous review of the preparation and properties of silver chloride electrodes can be found in [11].

To test silver chloride electrodes for DC recording, we investigated the properties of sharp (under 1 μm tip dimensions), silver-coated electrodes in terms of resistance and time constant, before and after chloriding. The electrodes were separated from the holding substrate and individual electrodes were wired and tested. An electrolyte solution droplet was generated at the tip of a syringe and the tips were immersed in the droplet. The surface tension of the droplet allows control over the length of the tip immersed (20–100 μm of the tip is estimated to be immersed in the solution).

The tips were dipped in solution and the DC resistance without chloride was initially 10–20 MΩ (corresponding to $\rho = 1\text{--}10 \times 10^9 \, \Omega \, \mu m^2$), with an approximately 5 ms time constant. However, these numbers began to rise almost instantly (<1 s) and the resistance rapidly became unmeasurably high, with a very long time constant (many seconds) and an unstable baseline.

Electrolytic chloride deposition on to the surface for a few seconds (9 V, with a 100 MΩ current limiting resistance), results in a new, stable DC potential level,

ie, a junction potential adjustment of –34 mV, which may simply indicate the removal of the previously unbalanced junction potential between the silver metal and the electrolyte. The new resistance, of the same electrode tip, will now measure about 20 MΩ (varying from 1 to 35 MΩ depending on the extent of the immersion of the tip). This value is fairly stable with a time constant of approximately 5 ms.

Further deposition (eg, 5 min, 9 V through 100 MΩ current-limiting resistance) results in a visible build-up of material on the tip (presumably, mostly chloride), a slightly reduced resistance, and an increase in the time constant.

The chloridation process yields electrodes with a significantly more stable baseline (±1 mV compared with >100 mV for non-chloride silver or gold). The measured resistance and capacitance for these electrodes ($R_{tip}=20$ MΩ, $C_{tip}=250$ pF) are in agreement with our estimates for the tips. These parameters are close to typical values of filled glass capillaries and may permit accurate DC recording.

1.3.3.5   Passivation Layer

To achieve insulation of the needle base we used a thin-film dielectric coating. Because of the topography and fragility of the sharp needles, sputtering deposition is advantageous over spinning of organic material. A convenient way to achieve insulation is by using sputtered silicon nitride. Owing to better durability, silicon nitride is better suited for such applications than silicon dioxide or polyimide [43, 44]. For better corrosion resistance and prolonged device lifetime, additional deposition material, such as triplex layers of silicon nitride and silicon dioxide, will be studied in the future [33]. To verify that our coatings are pinhole free we tested the nitride layers as a mask for aluminium etching. High-quality coatings were achieved for deposition at low background pressure.

1.3.3.6   Experimental Results

To test the performance of our electrodes we first used them in an extracellular preparation of *Manduca sexta* (hawk moth) (see Figure 1.3-11 a). *Manduca* is among the largest of flying insects; its flight control neural circuits are relatively well understood in the context of constrained laboratory environments. This insect has been studied extensively, including its flight dynamics, neuromuscular control, and visual and mechanosensory signaling [45].

A moth was anchored to a holder under a microscope and its lobula plate (the brain optic lobe) was exposed. A conducting wire was connected to the backside of a micro-machined needle device, and the needle was lowered into the lobula plate. A reference electrode was placed at a nearby position. In Figure 1.3-12 a
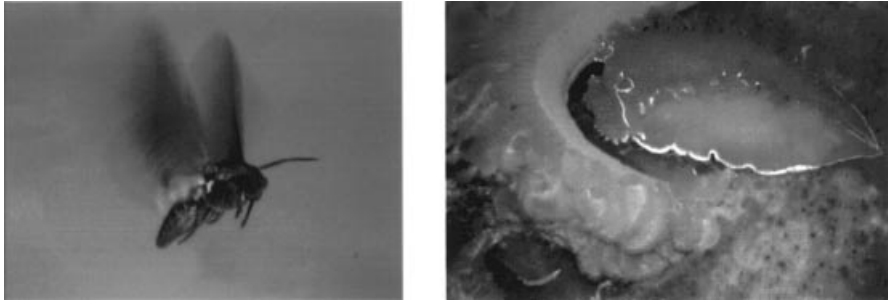
Figure 1.3-11. The biological models used in this work (**a**) *Manduca sexta* (hawk moth) is typically 4 cm in length with a 12 cm wingspan; at 2.5 g, it is among the largest of insect flyers. It can easily carry a test-electronics payload. (**b**) *Tritonia diomedea* (sea slug) is typically 20 cm in length, and has a readily accessible brain with large and well-characterized neurons (see Figure 1.3-1).

we show a record of the evoked extracellular potentials of one neuron in the lobula plate.

To test our gold-coated needles for intracellular applications we used the brain of *Tritonia diomedea* (a sea slug). Unlike the dry setup of the moth experiments, here the isolated brain was anchored in seawater under an optical microscope. An Ag/AgCl reference electrode was dipped in the seawater close to the brain. An insulated conducting wire was connected to the back of the micro-machined needle and the connection was insulated with varnish. At 100 Hz the electrode impedance was of the order of 1 MΩ.

Owing to the enormous dimensions of the sea slug brain cells ($\sim 400\ \mu$m), it is possible to monitor visually the penetration process and select an appropriate location for the probe as it approaches the cell. The micro-machined needles were mounted on a micro-manipulator and were slowly pressed against a cell membrane. Two effects were observed as the needles approached the cell: the measured background potential drifted and the membrane bent. After moderate tapping on the micro-manipulator, spikes were observed. This is probably due to cell membrane penetration. The recorded data are shown in Figure 1.3-13. Similar tests with dull electrodes (tip size $\sim 5\ \mu$m) did not result in signals with impulses.

The noise level seen in Figure 1.3-13 is due to induced 60 Hz interference and possibly to insufficient insulation and grounding of surrounding devices. Biofouling (the affinity of proteins to adhere to synthetic surfaces) may also contribute to the noise and the instability, which was observed in two separate tests of 1 h of recording. Finally, a damaged membrane is likely to contribute to the noise levels and to the relatively small amplitude and slow time constant signal seen in Figure 1.3-13.

The results presented so far show similarity between the geometry of the silicon needles and the pulled glass capillaries (see Figures 1.3-4 and 1.3-9) and support the potential for this process to produce intracellular silicon-based nee-
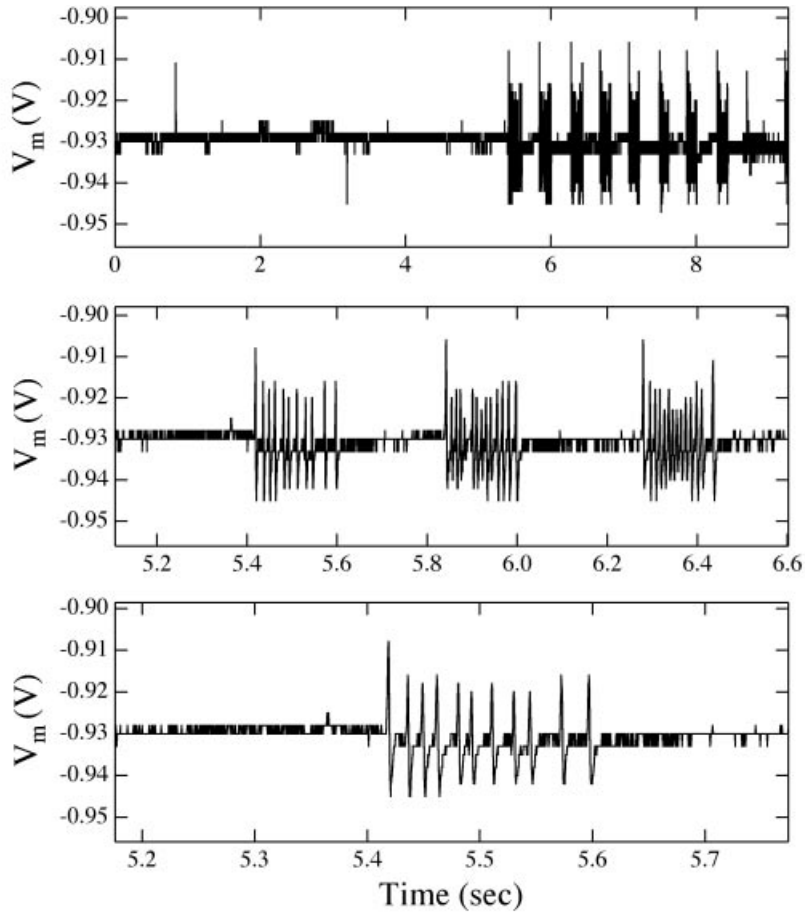
Figure 1.3-12. Evoked extracellular potentials in the lobula plate of *Manduca sexta* (hawk moth) plotted versus time (raw data).

dles. Further, the data in Figures 1.3-12 and 1.3-13 hint at the exciting possibilities for fully fledged neurobiological experiments using silicon-based electrodes.

1.3.3.7   Current and Future Work

The current design of our devices permits convenient handling by using the large base (Figure 1.3-10) to hold and manipulate the needles. During the measurements, however, when the needles are soaked in a conducting medium (eg, seawater or blood), the base acts as a large capacitor (impedance of $\sim 10\,\mathrm{M\Omega}$ at 100 Hz). This capacitor is in parallel with the active sensor (the tip of the nee-
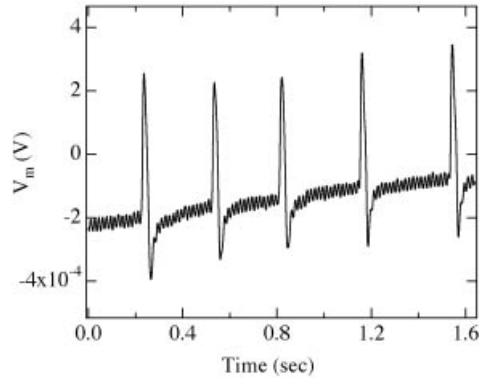
Figure 1.3-13. Recording results with an electrode coated with gold and insulated with nitride. Spontaneous intracellular potentials in a neuron in the brain of *Tritonia diomedea* (sea slug) plotted versus time. The positioning of the probe was controlled via micro-manipulators and an optical microscope.

dle) and can cut off valuable data. A better design should take this into account by limiting the dimensions of the base.

As a first step to improve our process, the dicing saw will be replaced with a deep reactive ion etching (DRIE) process. This will allow a versatile design of needle arrays. Future work will also focus on a versatile connectivity scheme. Preliminary work suggests that polyimide can be used as a convenient structural flexible connecting material. The qualities of the polyimide as a good ionic insulator can be employed to protect metallic lines, which will be used to connect the electrodes and to build large needle arrays. Finally, to enhance the electrode bio-compatibility a non-fouling coating will be deposited. Such a coating was recently tested for bio-MEMS applications and was verified to have good adhesion to silicon, nitride, and gold [9]. Also, it was found that this coating has good ionic conductivity.

1.3.4   Summary

We have reviewed the motivation and the main principles that underlie intracellular potential recording electrodes. We have presented a technique to produce sub-micrometer sharp, high aspect ratio silicon needles. With the refined geometry we were able to obtain high-quality *in vivo* extracellular recordings. Moreover, we presented the first evidence for cell penetration and recording with silicon needles inside a cell. With the advances in bio-MEMS along with the techniques discussed here, the long-term goals of our research are to build stand-alone implantable sensing units made of probes, amplifiers, and memory components, with the specific goal of allowing intracellular recording from freely behaving animals.

1.3.5   Acknowledgments

1.3.6   References

[1] Najafi, K., in: *Proceedings of the IEEE 6th International Symposium on Micro Machine and Human Science*; 1995, pp. 11–20.
[2] Della Santina, C.C., Kovacs, G.T.A., Lewis, E.R., *J. Neurosci. Methods* **72** (1997) 71–78.
[3] Bragin, A., Hetke, J., Wilson, C.L., Anderson, D.J., Engel J., Jr., Buzsáki, G., *J. Neurosci. Methods* **98** (2000) 77–82.
[4] Kandel, E.R., Schwartz, J.H., Jessell, T.M., *Principles of Neural Science*; Norwalk, CT: Appleton & Lange, 1991.
[5] Alberts, B., Bray, D., Lewis, J., Raff, M., Roberts, K., Watson, J.D., *Molecular Biology of the Cell*; Garland Publishing, New York, NY, 1994.
[6] Ogden, D., *Microelectrode Techniques, The Plymouth Workshop Handbook;* Cambridge: Company of Biologists, 1994.
[7] Shepherd, G.M., *Neurobiology*; Oxford: Oxford University Press, 1994.
[8] Brown, K.T., Flaming, D.G., *Neuroscience* **2** (1977) 813–827.
[9] Bard, J., Faulkner, L.R., *Electrochemical Methods*; New York: Wiley, 1980.
[10] Robinson, D.A., *Proc. IEEE* **56** (1968) 1065–1071.
[11] Geddes, L.A., *Electrodes and the Measurement of Bioelectric Events*; New York: Wiley, 1972.
[12] Kovacs, G.T.A., in: *Enabling Technologies for Cultured Neural Networks*, Stenger, D.A., McKenna, T.M. (eds.); San Diego: Academic Press, 1994, Chap. 7.
[13] Gesteland, R.C., Howland, B., Lettvin, J.Y., Pitts, W.H., *Proc. IRE* (1959) 1856–1862.
[14] Geddes, L.A., Baker, L.E., *Principles of Applied Biomedical Instrumentation*; New York: Wiley, 1968.
[15] Willows, A.O.D., *Science* **157** (1967) 570.
[16] Sze, S.M., *Semiconductor Sensors*; New York: Wiley, 1994.

[17] Kewley, D. T., Hills, M. D., Borkholder, D. A., Opris, I. E., Maluf, N. I., Storment, C. W., Bower, J. M., Kovacs, G. T. A., *Sens. Actuators A* **58** (1997) 27–35.

[18] Wise, K. D., Angell, J. B., Starr, A., presented at the 8th International Conference on Medical and Biological Engineering, 1969.

[19] Blum, N. A., Carkhuff, B. G., Charles, H. K., Edwards, R. L., Meyer, R., *IEEE Trans. Biomed. Eng.* **38** (1991) 68–74.

[20] Ensell, G., Banks, D. J., Ewins, D. J., Balachandran, W., Richards, P. R., *J. Microelectromech. Syst.* **5** (1996) 117–121.

[21] Rutten, W. L. C., van- Wier, H. J., Put, J. H. M., *IEEE Trans. Biomed. Eng.* **38** (1991) 192.

[22] Papageorgiou, D., Bledsoe, S. C., Gulari, M., Hetke, J. F., Anderson, D. J., Wise, K. D., presented at the 14th IEEE International Conference on Micro Electro Mechanical Systems, 2001.

[23] Chen, J., Wise, K. D., *IEEE Trans. Biomed. Eng.* **44** (1997) 770.

[24] Kristensen, B. W., Noraberg, J., Thiébaud, P., Koudelka-Hep, M., Zimmer, J., *Brain Res.* **896** (2001) 1–17.

[25] Horbett, T. A., in: *Biomaterials: Interfacial Phenomena and Applications*, Cooper, S. L., Peppas, N. L. (eds.); Washington DC: American Chemical Society, 1982, p. 233.

[26] Costerton, J. W., Stewart, P. S., *Sci. Am.* **285** (2001) 75–81.

[27] Zhang, M., Desai, T., Ferrari, M., *Biomaterials* **19** (1998) 953–960.

[28] Auerbach, H., Soller, B. R., Peura, R. A., in: *Proceedings of the 20th Annual Northeast Bioengineering Conference*; 1994, pp. 108–109.

[29] Yang, Y., Zhang, S. F., Kingston, M. A., Jones, G., Wright, G., Spencer, S. A., *Biosens. Bioelectron.* **15** (2000) 221–227.

[30] Choi, E. T., Callow, A. D., in: *Implantation Biology: the Host Response and Biomedical Devices*, Greco, R. S. (ed.); Boca Raton, FL: CRC Press, 1994, Chap. 3.

[31] Stelzle, M., Wagner, R., Jagermann, W., Fröhlich, R., in: *Proceedings of the 18th Annual International Conference of the IEEE*; 1997, Vol. 1, p. 114.

[32] Hanein, Y., Pan, Y. V., Ratner, B. D., Denton, D. D., Böhringer, K. F., *Sens. Actuators B* (2001). in press

[33] Fassbender, F., Schmitt, G., Schöning, M. J., Luth, H., Buss, G., Schultze, J. W., *Sens. Actuators B* **68** (2000) 128–133; Schmitt, G., Schultze, J. W., Fassbender, F., Buss, G., Lüth, H., Schöning, M. J., *Electrochim. Acta* **44** (1999) 3865–3883.

[34] Regehr, W. G., Pine, J., Rutledge, D. B., *IEEE Trans. Biomed. Eng.* **35** (1998) 1023–1032.

[35] Grattarola, M., Martinoia, S., *IEEE Trans. Biomed. Eng.* **40** (1993) 35–41.

[36] Buitenweg, J. R., Rutten, W. L. C., Marani, E., in: *Proceedings of the 22nd Annual International Conference of the IEEE Engineering in Medicine and Biology Society*; (2000) 2004–2007.

[37] Buzsaki, G., Kandel, A., *J. Neurophysiol.* **79** (1998) 1587–1591.

[38] Campbell, P. K., Jones, K. E., Huber, R. J., Horch, K. W., Norman, R. A., *IEEE Trans. Biomed. Eng.* **38** (1991) 758–768.

[39] Thiébaud, P., Beuret, C., Koudelka-Hep, M., Bove, M., Martinoia, S., Grattarola, M., Jahnsen, H., Rebaudo, R., Balestrino, M., Zimmer, J., Dupont, Y., *Biosens. Bioelectron.* **14** (1999) 61–65.

[40] Chun, K., Hashiguchi, G., Toshiyoshi, H., Fujita, H., Kikuchi, Y., Ishikawa, J., Murakami, Y., Tamiya, E., in: *Technical Digest of IEEE International Conference on MEMS*; (1999) 406–411.

[41] Bengtsson, M., Wallman, L., Drott, J., Laurell, T., in: *Proceedings of the 20th Annual International Conference of the IEEE Engineering in Medicine and Biology Society*; 1998, p. 2229.
[42] Griss, P., Enoksson, P., Stemme, G., in: *Proceedings of the 14th IEEE International Conference on Micro Electro Mechanical Systems*; 2001, p. 46.
[43] Frazier, A.B., O'Brien, D.P., Allen, M.G., in: *Proceedings of the IEEE International Conference on Micro Electro Mechanical Systems;* (1993) 195–200.
[44] James, K.J., Norman, R.A., in: *Proceedings of the 16th Annual International Conference of the IEEE*; 1994, pp. 836–837.
[45] Moreno, C.A., Tu, M.S., Daniel, T.L., *Am. Zool.* **40** (2000) 1138–1139.

List of Symbols and Abbreviations

Symbol	Designation
A	area
A_{Base}	area of passivation layer
A_{tip}	tip area
r	radius
C_d	glass wall capacitance
C_e	electrode capacitance
C_{tip}	tip capacitance
d	thickness of passivation layer
F	Faraday constant
f	frequency
h	height
i	induced current
i_0	exchange current density
l	length
L	length
R	gas constant
R_e	electrode resistance
R_{tip}	tip resistance
T	temperature
V_e	electrode voltage
V_m	resting membrane potential
ΔV	applied potential
a	angle
ε_0	dielectric permittivity of free space
ε_r	relative dielectric permittivity of passivation layer
ρ	resistivity

Abbreviation	Explanation
DRIE	deep reactive ion etching
fMRI	functional magnetic resonance imaging
MEA	microelectrode array
MEMS	microelectromechanical systems
PET	positron emission tomography
RIE	reactive ion etching
ESEM	Environmental scanning electron microscope